Journal of Alloys and Compounds 501 (2010) 54–59

Contents lists available at ScienceDirect

Journal of Alloys and Compounds

journal homepage: www.elsevier.com/locate/jallcom

Characteristics of doped TiO_2 photocatalysts for the degradation of methylene blue waste water under visible light

Zhongqing Liu[a,b,*], Yicao Wang[b], Wei Chu[a], Zhenhua Li[b], Changchun Ge[b]

[a] School of Chemical Engineering, Sichuan University, Chengdu 610065, China
[b] School of Materials Science and Technology, University of Science and Technology Beijing, Beijing 100083, China

ARTICLE INFO

Article history:
Received 6 January 2010
Received in revised form 29 March 2010
Accepted 2 April 2010
Available online 10 April 2010

Keywords:
N-doped TiO_2 catalyst
Photocatalytic degradation
Electron structure
Density functional simulation
Density of states (DOS)

ABSTRACT

Fe-doped, N-doped, (Fe,N)-codoped and undoped TiO_2 were prepared by a hydrothermal treatment, followed by a calcination process, using $TiOSO_4$, $CO(NH_2)_2$ and $Fe(NO_3)_3$ as raw materials. The samples were characterized by XRD, XPS, TEM, PL, FT-IR and UV-Vis diffuse reflectance spectra. Photocatalytic experiments were carried out by decomposition of methylene blue aqueous solution under visible light. It was found that as-prepared TiO_2-based catalysts were single phasic anatase titania. Among these samples, the N-doped TiO_2 exhibited the better photocatalytic activity. The relations of their photocatalytic activity, spectroscopy properties and band gap structures have been discussed while *ab initio* calculations of electron structure and density of state (DOS) were done by DFT quantum chemistry method.

1. Introduction

In recent years, TiO_2-based catalysts have attracted increasing attentions due to their prominent application prospects in the areas of degradation of pollutants in water and air, photoelectrochemical splitting of water and photoelectric conversion. Unfortunately, TiO_2 exhibits catalytic activity only under ultraviolet light because it has a band gap of 3.2 eV, failing to use visible light accounting for near 50% of sunlight spectrum. Therefore, a large amount of investigations aiming at narrowing band gap of TiO_2 to response to visible light have been carried out, using dopants. Up to now, several types of dopants, including transitional metal ions, alkali metal additives, nonmetal promoters as well as metal and nonmetal co-dopants (such as La/Sr and N) have been studied to prepare codoped TiO_2 photocatalysts. Among metal dopants, Fe (β) has been thought to be an excellent dopant [1–7] because doped Fe^{3+} replaces Ti^{4+} in TiO_2 lattice, forming localized bands near the bottom of conduction band and thereby decreasing band gap. For nonmetal dopants, N is found to be an outstanding candidate, in respect that doped N can not only broaden wavelength responded scope but also not debase photocatalytic activity under ultraviolet light [8–15]. However, TiO_2 photocatalysts codoped with metal ions such as Fe^{3+} and nometal species such as N have been few researched [16–18]. In our previous work [17], although (metal, N)-codoped TiO_2 catalysts have been fabricated by sol-gel auto-ignition route, they are mixed phases with anatase and rutile due to a high preparation temperature close to 1000 °C in auto-ignition process. In present work, a different preparation method was used to prepare TiO_2-based photocatalysts with a single phasic anatase. The relations of photocatalytic activity, spectroscopy properties and band gap structures of the catalysts have been discussed while *ab initio* calculations of electron structures were carried out by DFT method.

2. Experimental

$TiOSO_4$, $CO(NH_2)_2$ and $Fe(NO_3)_3$ with chemical grade, were used in our experiments without further purification. In a typical process, solution of $TiOSO_4$ and $CO(NH_2)_2$ was moved into a 500 mL Teflon-lined stainless autoclave. The concentration of $TiOSO_4$ was 0.5 mol L^{-1} and the molar ratio of $TiOSO_4$ to $CO(NH_2)_2$ was 1:5. After the autoclave was sealed, it was heated at 160 °C for 6 h. Subsequently, the product was taken out and washed with distilled water and absolute ethanol repeatedly to make $TiO_2 \cdot nH_2O$ free of sulphate ions. To fabricate undoped TiO_2 powders, the washed product was dried in an oven at 120 °C for 12 h and calcined at 500 °C for 2 h in a muffle furnace under an aerated condition. To prepare N-doped TiO_2 catalyst, the dried TiO_2 powders from hydrothermal process were mixed with $CO(NH_2)_2$ at a molar ratio of 1:1 before they were calcined at 500 °C for 2 h. Correspondingly, Fe-doped TiO_2 was prepared by adding $Fe(NO_3)_3$ to the solution of $TiOSO_4$ and $CO(NH_2)_2$ before hydrothermal treatment. (Fe,N)-codoped TiO_2 was synthesized using the same conditions and procedure as that of preparing N-doped TiO_2 except for that $Fe(NO_3)_3$ was added to the solution of $TiOSO_4$ and $CO(NH_2)_2$ prior to hydrothermal treatment. The quantity of $Fe(NO_3)_3$ was 1.0 at.% according to the formula: $M_{Fe}/(M_{Fe} + M_{Ti})$, where M_{Fe} and M_{Ti} were mole number of $Fe(NO_3)_3$ and $TiOSO_4$ used in our experiments, respectively.

* Corresponding author at: School of Chemical Engineering, Sichuan University, Chengdu 610065, China. Tel.: +86 21 8540 0422; fax: +86 21 8540 0422.
E-mail address: 301qzl@vip.sina.com (Z.Q. Liu).

0925-8388/$ – see front matter © 2010 Elsevier B.V. All rights reserved.
doi:10.1016/j.jallcom.2010.04.027

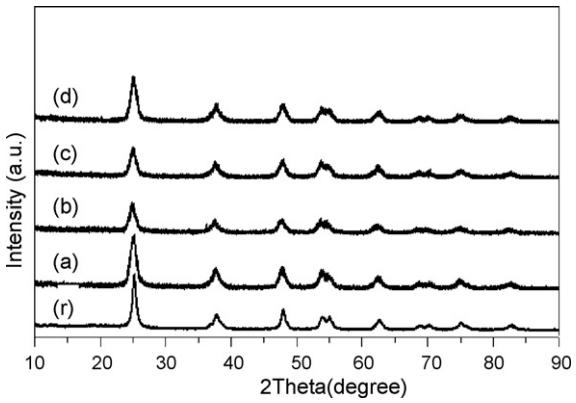

Fig. 1. XRD patterns of (r) anatase titania, (a) undoped TiO_2, (b) N-doped TiO_2, (c) Fe-doped TiO_2 and (d) (Fe,N)-codoped TiO_2.

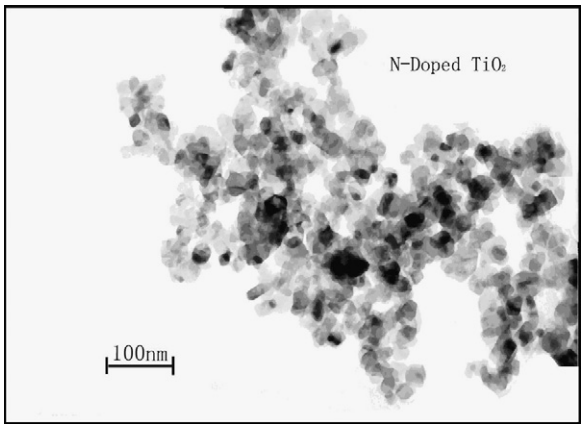

Fig. 2. TEM image of the N-doped TiO_2 powders.

The samples were characterized by several techniques: X-ray powder diffraction (XRD; Rigaku D/Max-RB, Japan) with CuK_α radiation ($\lambda = 0.15406$ nm), X-ray photoemission spectroscopy (XPS, VG ESCALAB, MKII UK) with MgK_α as an excitation source (the XPS peak positions of each element were corrected by using of C 1s (284.6 eV), UV-Vis diffuse reflectance spectrum with $BaSO_4$ as a substrate, Fluorescence spectra photometer (F-4500) with an excitation wavelength of 340 nm, Transmission electron microscopy (Philips EM400T apparatus) (TEM), and FT-IR using KBr flakes (NEXUS470 spectrophotometer). Identical experiments were also carried out with anatase titania (PW 25, purity ≥ 99%) for comparison.

Photocatalytic activity of the samples was investigated by decomposition of methylene blue (hereafter abbreviated as MB) aqueous solution under illumination of electron saving-energy lamp with major emission at 545 nm (Philips, YPZ 220/14-2U.RR.D, 14 W, 760 lm, 23.73 mW/cm^2). The initial concentration of MB was 10 mg L^{-1}. The dosage of the TiO_2 powders was 0.5 g for 500 mL MB solution with the pH value of 7.0. Before switching on irradiation, MB solution was continuously stirred in the dark for 1 h to ensure adsorption–desorption equilibrium. The solution samples were collected from the reactor at regular intervals, centrifuged and analyzed to determine the amounts of residual MB after photo-irradiation, using UV-Vis spectro-photometer (Unico 7200).

The $2 \times 2 \times 1$ TiO_2 supercells that possess an anatase crystal structure, $Ti_{16}O_{32}$, $Ti_{16}O_{31}N$, $Ti_{15}FeO_{32}$ and $Ti_{15}FeO_{31}N$, were used for the calculations of electronic structures. The calculations were performed using CASTEP software in Accelrys MS Modelings 3.1 package, in which the GGA and PW91 were introduced for the exchange-correlation function. Meanwhile, ultra-soft pseudo-potential was employed with cut-off energy of 340 eV and reciprocal-space integration over the irreducible Brillouin Zone was approximated at a finite number of k-points using the Monkhorst–Pack scheme with $3 \times 3 \times 2$ k-points grid. The lattice parameters and atomic positions of the supercells were optimized by minimizing the total energy before the calculations of the electronic structures.

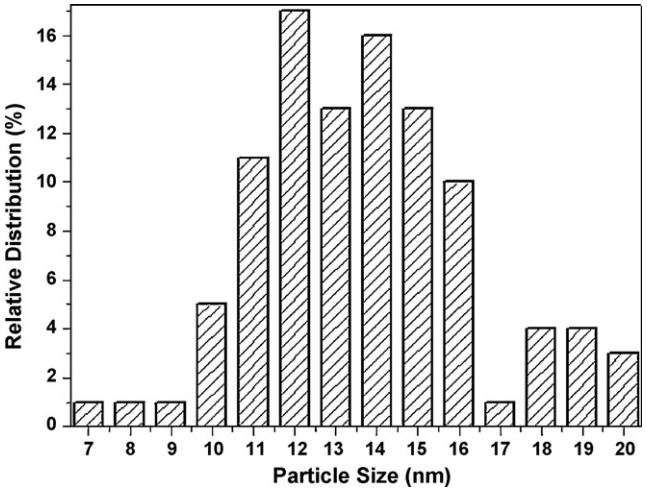

Fig. 3. Particle size distribution histogram of the N-doped TiO_2.

3. Results and discussion

X-ray diffraction is a method of long-order characterization of solids and heterogeneous catalysts, by which phase composition can be identified and particle size can be estimated using Scherrer equation [19]. XRD patterns of the TiO_2-based powders are shown in Fig. 1. The respective average crystallite size obtained with the help of the Scherrer equation is 8–10 nm. It is noticeable that for the N-doped TiO_2, the height of the main diffraction peak (1 0 1) is the lowest of these samples, indicating that it possesses smaller crystallite size. As a representative, TEM image of the N-doped TiO_2 is given in Fig. 2. The particle size distribution data generated from the TEM micrographs by inspection of 100 particles is shown in Fig. 3. The histogram confirms that most of the particles range from 11 to 16 nm. This is greater than the average crystallite size (8–10 nm) attained from the XRD, which may be caused by their heterocrystal structure. The XRD patterns are found to match that of the anatase phase (JCPDS 21-1272). No peaks corresponding to oxides of iron is observed, such as Fe_xO_y, Fe_xN_y and $Fe_xN_yO_z$. Therefore, it can be inferred that either iron ions have been substituted into the crystallite lattice sites of titania or iron oxides exist as a highly dispersed polymeric form over surface, which cannot be detected by XRD [20]. To clarify

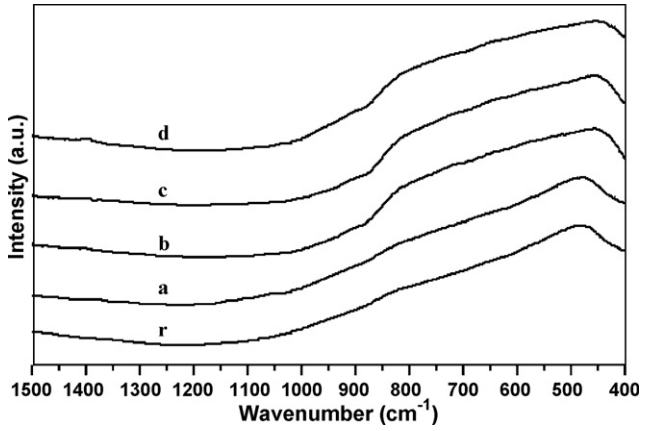

Fig. 4. FT-IR spectra of (r) anatase titania, (a) undoped TiO_2, (b) N-doped TiO_2, (c) Fe-doped TiO_2 and (d) (Fe,N)-codoped TiO_2.

the state of the doped iron ions, Fourier transform infrared spectra of the PW25 and the as-prepared TiO_2 were conducted. It can be seen that in Fig. 4 the FT-IR spectra have identical characteristics, exhibiting a distinct broadband in the 400–900 cm^{-1} region, which have been assigned to bending vibrations of the Ti–O–Ti bond of anatase titania. There is no separate sharp peak at around 1223 cm^{-1} that is a signature peak of the Fe^{3+}–O^{2-} stretch in Fe_2O_3 [21]. Based on the results, it can be concluded that iron is

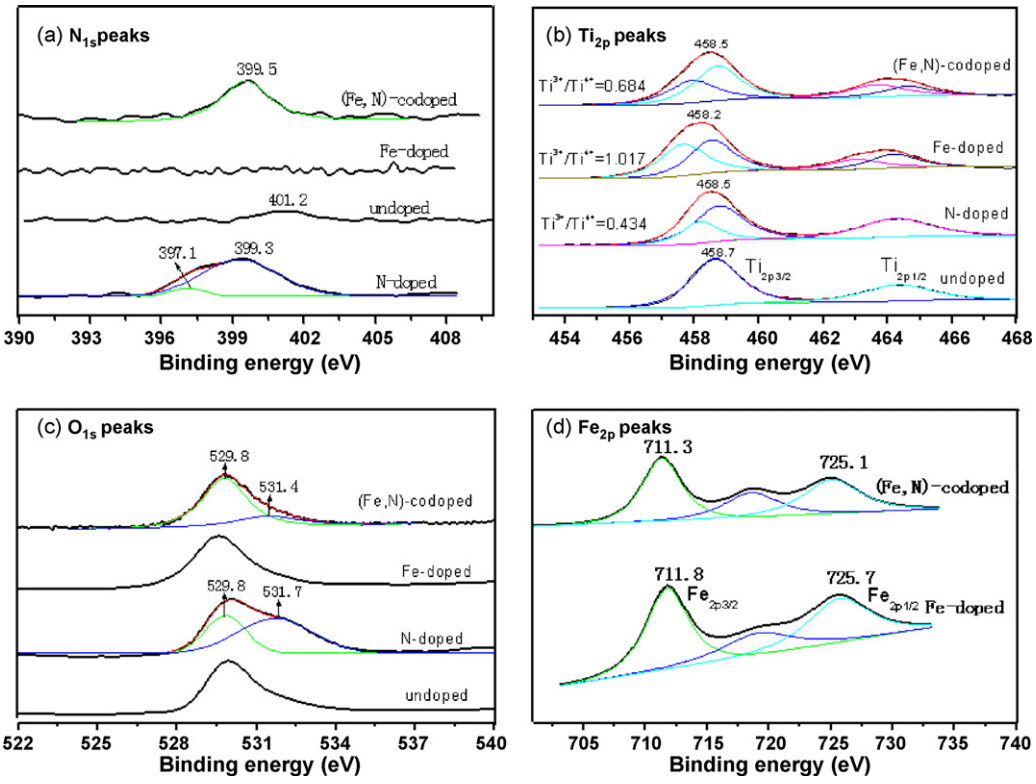

Fig. 5. XPS spectra of the elements for the as-prepared powders: (a) N 1s peaks, (b) Ti 2p peaks, (c) O 1s peaks and (d) Fe 2p peaks.

doped in the lattice sites of the TiO_2 instead of being a separate entity.

In order to check if nitrogen species have been doped into the N-doped and (Fe,N)-codoped TiO_2, XPS measurements were carried out. It is obvious that in Fig. 5(a) no N 1s peak is detected for the Fe-doped TiO_2, while for undoped TiO_2 only one weak N 1s peak at 401.2 eV is observed. For N-doped TiO_2, there is a strong peak of N 1s at the centre position of 398.2 eV, which can be fitted into two peaks at 397.1 and 399.3 eV, corresponding nitrogen mol percentage calculated from the XPS is 5.70 at%. For (Fe,N)-codoped TiO_2, N 1s peak appeared at 399.5 eV, the nitrogen mol percentage is 4.84 at%. Asahi and co-workers reported N 1s peak at 396 eV would appear in the XPS spectra when N replaced O at oxygen sites in TiO_2 lattice and the peak at 400 eV should be assigned to NH_3 or N-containing organic compounds adsorbed on TiO_2 [10]. Additionally, it was proposed that O–Ti–N had been formed when N 1s binding energy shifted to position higher than 396 eV and lower than 400 eV [23,24]. Therefore, the Ti $2p_{3/2}$ peak shift of 0.2 eV toward lower binding energy compared to the undoped TiO_2 should be ascribed to the formation of O–Ti–N bond for the N-doped TiO_2 and the (Fe,N)-codoped TiO_2, where N atoms replaced O atoms at oxygen sites in TiO_2 lattice. In addition, the asymmetry in the Ti $2p_{3/2}$ peak on the lower binding energy side for the doped TiO_2 and O 1s peaks for the N-doped and (Fe,N)-codoped TiO_2 indicates interaction between either Fe or N and TiO_2. The effects of non-stoichiometry can be represented schematically by the following reactions, where V_e and V_h express vacancies of anions and cations respectively.

$$Fe^{3+} + Ti^{4+} + 2O^{2-} \rightarrow Fe^{3+}\tfrac{3}{2}O^{2-}\tfrac{1}{2}V_e + O^{2-} + Ti^{4+} \quad (1)$$

$$N^{3-} + Ti^{4+}2O^{2-} \rightarrow \tfrac{3}{4}Ti^{4+}N^{3-}\tfrac{1}{4}V_h + 2O^{2-} + \tfrac{1}{2}Ti^{4+} \quad (2)$$

The O 1s peak at lower binding energy is due to the O^{2-} anions (Fig. 5(c)), while the shoulder peak at higher binding energy should be attributed to surface hydroxyl groups or chemisorbed water molecules [9]. Correspondingly, the Ti 2p peak at lower binding energy should be ascribed to Ti^{3+}, while the peak at higher binding energy is assigned to the Ti^{4+}. It can be seen that the ratio of Ti^{3+}/Ti^{4+} for the (Fe,N)-codoped TiO_2 is the lowest among the doped samples, indicating the interaction between the doped additives as follows.

$$xFe^{3+} + yN^{3-}2O^{2-} + Ti^{4+} \rightarrow xFe^{3+}\tfrac{3x}{2}O^{2-}\tfrac{3y}{4}Ti^{4+}yN^{3-}\left(\tfrac{y}{4}V_h\tfrac{x}{2}V_e\right) + (2-x)O^{2-} + \left(1-\tfrac{y}{2}\right)Ti^{4+} \quad (3)$$

In Fig. 5(d), the binding energies from 711.3 to 711.8 eV and from 725.1 to 725.7 eV should be assigned to $2p_{3/2}$ and $2p_{1/2}$ of Fe^{3+}, respectively, which exhibits a positive shift compared to those in Fe_2O_3 (710.7 eV for $2p_{3/2}$ and 724.3 eV for $2p_{1/2}$). The slight enhancement of Fe 2p level binding energy should be attributed the diffusion of Fe^{3+} into TiO_2 lattice and the formation of Fe-O-Ti bond in the Fe-doped and (Fe,N)-codoped TiO_2 [4,22]. Using the formula $M_1 = (A_1/\alpha_1)/\sum_1^n A_i/\alpha_i$ (where A_i, α_i expressed area of XPS peaks, sensitivity factor of i element, respectively) and making a conversion to weight percentage, Fe concentration of the Fe-doped and (Fe,N)-codoped TiO_2 is 1.11, 1.19 wt.% respectively.

Fig. 6 depicts UV-Vis diffuse absorptance spectra of the samples. Obviously, absorption threshold edges of the samples are shifted better into the visible light region except for the undoped TiO_2, with a stronger absorption in the visible light region from 400 to 500 nm. As it is well known, for direct band gap semiconductor such as TiO_2, that onset of light absorption can be estimated by plots of $(\alpha h\nu)^2$ versus photon energy [23,24]. The direct band gap energies estimated from intercept of tangents of the plots were 3.22, 3.18, 3.11 and 3.07 eV for the undoped, N-doped, Fe-doped and (Fe,N)-codoped TiO_2, respectively. Among these samples, the optical band gap of the (Fe,N)-codoped TiO_2 is the lowest. The reason should be contributed to the simultaneous substitutions of Fe^{3+} for Ti^{4+}

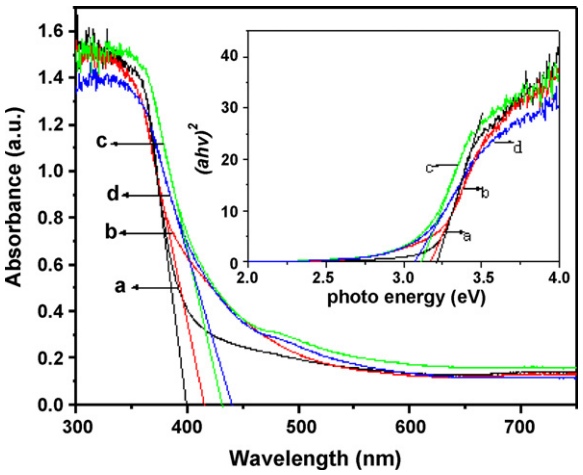

Fig. 6. UV–vis diffuse absorptance spectra of the samples. (a) undoped, (b) N-doped, (c) Fe-doped and (d) (Fe,N)-codoped TiO_2. The inset was the plots of $(\alpha hv)^2$ versus photon energy for direct transition.

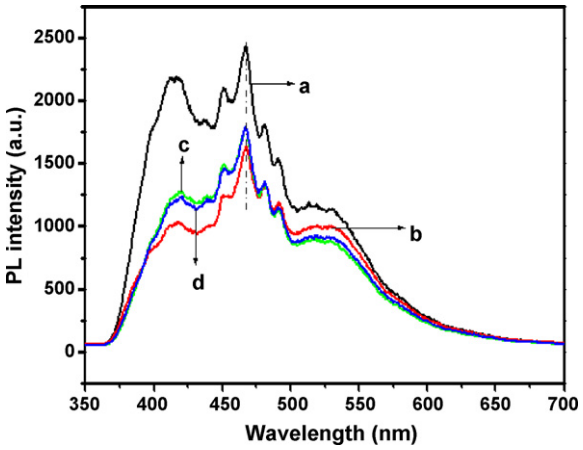

Fig. 7. PL spectra of the samples. (a) undoped, (b) N-doped, (c) Fe-doped and (d) (Fe,N)-codoped TiO_2.

and N^{3-} for O^{2-}, not only forming localized bands via Fe 3d at the bottom of conduction band but also hybrid bands via N 2p and O 2p close to the top of valence band.

The photoluminescence (PL) spectra of the specimens are shown in Fig. 7. From the shape and position of the PL emission peaks, there is no evident difference, but their relative intensities exhibit remarkable differences between the undoped TiO_2 and doped TiO_2. The PL intensity of the doped TiO_2 is lower than the undoped TiO_2. It is well known that PL spectrum of nanostructure materials is related to its transfer behavior of photo-induced electrons and holes, reflecting the separation and recombination of charge carriers [25–27]. For the N-doped TiO_2, its PL intensity is the weaker among the four samples. Thus, recombination rate of charge carriers is the lower, whereas that of the undoped TiO_2 is higher due to its stronger PL intensity. PL spectra of the Fe-doped TiO_2 and the (Fe,N)-codoped TiO_2 are nearly consistent and both higher than that of the N-doped TiO_2.

The results of photocatalytic experiments are given in Fig. 8. The N-doped TiO_2 presents the better photocatalytic activity and the (Fe,N)-codoped TiO_2 is only better than the undoped TiO_2. The apparent kinetic constant of the (Fe,N)-codoped TiO_2 fitted from $\ln(C_0/C_t) \sim t$ curve is 0.1694 h^{-1} (where C_0 is MB initial concentration, C_t is MB concentration at the t moment, t is irradiation time). The value is higher than that of the undoped TiO_2 (0.0829 h^{-1}), slightly lower than that of the Fe-doped TiO_2 (0.1975 h^{-1}) and

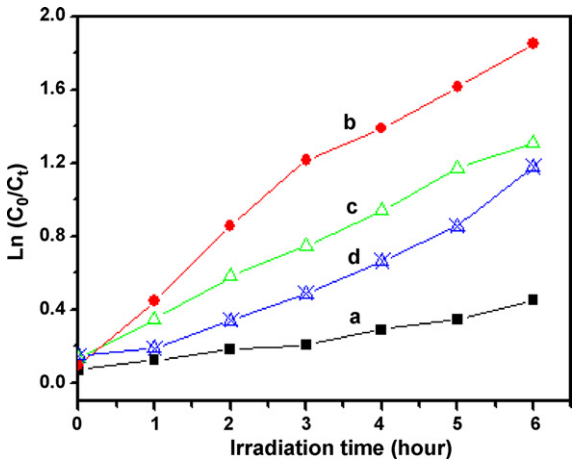

Fig. 8. Photocatalytic degradation of MB under visible light. (a) undoped, (b) N-doped, (c) Fe-doped and (d) (Fe,N)-codoped TiO_2.

much lower than that of the N-doped TiO_2 (0.2774 h^{-1}). These experimental results will be discussed by combining the theoretical simulations below.

The first-principle calculation, because it can provide the information on structure of band gap and density of state (DOS), has been proved to be one of the most powerful tools to evaluate catalysts [28–33]. The total and partial DOS of undoped, N-doped, Fe-doped and (Fe,N)-codoped TiO_2 with anatase crystal structure ($I41/amd$ space group, $a = 7.568$ Å, $c = 9.515$ Å, for $2 \times 2 \times 1$ super cell) are presented in Fig. 9, where the Fermi energy (E_F) locates at zero on the energy axis. It can be seen that the 3d orbits are mainly responsible for conduction bands and 2p orbits for valence bands, while the state of valence band maximum (hereafter denoted as VBM) and band gap are obviously different. For N-doped TiO_2, a hybrid energy level is formed at VBM due to substitution N^{3-} for O^{2-}, resulting in that the bang gap is narrowed, with a continuum of state at VBM formed, this is crucial for enhancement of photocatalytic efficiency [10]. For (Fe,N)-codoped TiO_2 (Fig. 7(d)), although local bands are formed by Fe 3d at near Fermi energy as Fe-doped TiO_2, their overlap degree with O 2p is significantly increased, nearly arriving at a complete overlap of DOS between Fe 3d and O 2p at VBM, along with a reformation of valence and conduction band edges. As a result, a higher cleavage of valence and conduction band edges is conducted and band gap is further decreased. In contrast, for Fe-doped TiO_2 (Fig. 7(c)), there is few DOS overlap between Fe 3d and O 2p at VBM, where the detached energy level is formed by Fe 3d. These suggest that shallow traps should be formed for the Fe-doped TiO_2 and the N-doped TiO_2 respectively, this is beneficial to promoting efficient separation of photo-induced charge carries. Correspondingly, for (Fe,N)-codoped TiO_2, deeper traps are constructed and at VBM, where there are recombination traps for h^+:

$$Fe^{3+}h^+ \rightleftarrows Fe^{4+} \quad (4)$$

$$N^{3-} + h^+ \rightleftarrows N^{2-} \quad (5)$$

$$Fe^{3+}(e^-) + N^{3-}(h^+) \rightarrow Fe^{3+}N^{3-} + E_h \quad (6)$$

Accordingly, a recombination center with high efficient rate is formed and photo-generated holes are remarkably localized. This significantly retards speedy transfer and separation of trapped electron-hole pairs and greatly increases recombination possibility of photo-induced carries. This is the reason the (Fe,N)-codoped TiO_2 possesses the strongest PL intensity, because the majority of photo-generated electrons and holes are re-combined in its deep traps formed the additives of Fe and N. It is true that, in the photocatalytic process, the non-stoichiometric effects have a certain role.

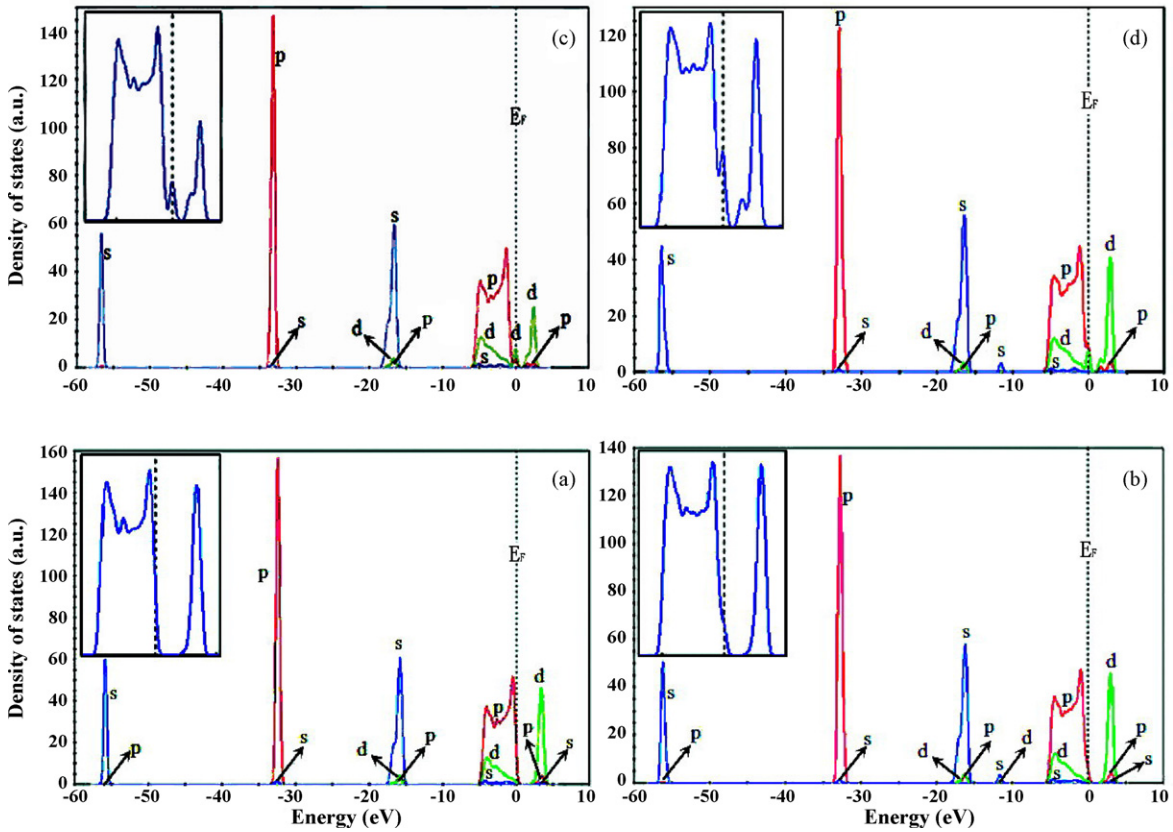

Fig. 9. Density of states (DOS) of the four models. (a) undoped, (b) N-doped, (c) Fe-doped and (d) (Fe,N)-codoped TiO_2. The insets showed the magnified partial DOS near Fermi energy level.

Nevertheless, the effective radical concentration is lower because the most h^+ are quenched by Fe^{3+} and N^{3-} in the migration process to the catalyst surface, therefore, there are not enough h^+ to activate oxygen anions or hydroxyls produced by non-stoichiometric effects on the catalyst surface. It is not difficult to explain that the (Fe,N)-codoped TiO_2 possesses the lowest band gap, but its photocatalytic activity is very low, only higher than the undoped TiO_2. This is different from either the (Sr, N)-codoped TiO_2 or the (La, N)-codoped TiO_2 [16,17,34,35], which shows an enhanced photocatalytic activity. The possible reason should be ascribed that ion radius of Sr^{3+} or La^{3+} is greater than Ti^{4+}, it cannot substitute for Ti^{4+} and enter into the TiO_2 lattice. Thus, double substitution doping of N for O and Sr for Ti, as well as N for O and La for Ti cannot make it, deep traps are not be formed yet. In this case, the doped Sr^{3+} or La^{3+} exists as a highly dispersed polymeric form and changes the transmission path of photo-generated electrons. Consequently, the separation of photo-induced charge carries is accelerated and photocatalytic activity is enhanced.

4. Conclusions

TiO_2-based photocatalysts with single phasic anatase, including undoped, N-doped, Fe-doped and (Fe,N)-codoped TiO_2 were successfully prepared. The relations of their photocatalytic performances and spectroscopy properties as well as the results of PL spectra have been investigated and discussed while the DOS calculation was carried out. The (Fe,N)-codoped TiO_2 possesses the narrower band gap, higher PL signal intensity and deeper traps than the N-doped TiO_2 and the Fe-doped TiO_2, which tends to forming deep capture of charge carries. Accordingly, photocatalytic activity of the (Fe,N)-codoped TiO_2 is only higher than the undoped TiO_2, slightly lower than the Fe-doped TiO_2 and much lower than the N-doped TiO_2. The N-doped TiO_2 catalyst with single phasic anatase presents the better photocatalytic activity under visible light.

Acknowledgement

The work was financially supported by the National Natural Science Foundation of China (grant no. 50774053).

References

[1] Y.M. Wu, J.L. Zhang, L. Xiao, F. Chen, Appl. Catal. B Environ. 88 (2009) 525–532.
[2] C. Adan, J. Carbajo, A. Bahamonde, A. Martinez-Arias, Catal. Today 143 (2009) 247–252.
[3] F. Lin, D.M. Jiang, X.M. Ma, J. Alloys Compd. 470 (2009) 375–378.
[4] Y.F. Tu, S.Y. Huang, J.P. Sang, X.W. Zou, Mater. Res. Bull. 45 (2010) 224–229.
[5] P. Vijayan, C. Mahendiran, C. Suresh, K. Shanthi, Catal. Today 141 (2009) 220–224.
[6] E. Thimsen, S. Biswas, C.S. Lo, P. Biswas, J. Phys. Chem. C 113 (2009) 2014–2021.
[7] J. Zhu, J. Ren, Y.N. Huo, Z.F. Bian, H.X. Li, J. Phys. Chem. C 111 (2007) 18965–18969.
[8] J.H. Yan, Y.R. Zhu, Y.G. Tang, S.Q. Zheng, J. Alloys Compd. 472 (2009) 429–433.
[9] F. Dong, W.R. Zhao, Z.B. Wu, S. Guo, J. Hazard. Mater. 162 (2009) 763–770.
[10] R. Asahi, T. Morikawa, T. Ohwaki, K. Aoki, Y. Taga, Science 293 (2001) 269–271.
[11] S. Livraghi, A.M. Czoska, M.C. Paganini, E. Giamello, J. Solid State Chem. 182 (2009) 160–164.
[12] Y.L. Hu, H.F. Liu, W.R. Chen, D.B. Chen, J.W. Yin, X.P. Guo, J. Nanosci. Nanotechnol. 10 (2010) 2232–2237.
[13] C. Kim, M. Choi, J. Jang, Catal. Commun. 11 (2010) 378–382.
[14] G.H. Tian, Y.J. Chen, K. Pan, D.J. Wang, W. Zhou, Z.Y. Ren, H.G. Fu, Appl. Surf. Sci. 256 (2010) 3740–3745.
[15] S. Livraghi, M.R. Chierotti, E. Giamello, G. Magnacca, M.C. Paganini, G. Cappelletti, C.L. Bianchi, J. Phys. Chem. C 112 (2008) 17244–17252.
[16] H.Y. Wei, Y.S. Wu, N. Lun, F. Zhao, J. Mater. Sci. 39 (2004) 1305–1308.
[17] Z.Q. Liu, Y.P. Zhou, Z.H. Li, Y.C. Wang, C.C. Ge, Rare Met. 26 (2007) 263–270.
[18] S. Yoshiaki, A. Hiroyuki, O. Kensen, K. Hironobu, N. Jun, T. Tsuyoshi, K. Junko, N.H. Michikazu, D. Kazunari, J. Mater. Res. 19 (2004) 2100–2108.
[19] A.Y. Khodakov, W. Chu, P. Fongarland, Chem. Rev. 107 (2007) 1692–1744.
[20] K. Bhattacharyya, S. Varma, A.K. Tripathi, S.R. Bharadwaj, A.K. Tyagi, J. Phys. Chem. C 112 (2008) 19102–19112.

[21] M. Zic, M. Ristic, S. Music, J. Mol. Struct. 924–926 (2009) 235–242.
[22] J.F. Zhu, F. Chen, J.L. Zhang, H.J. Chen, M. Anpo, J. Photochem. Photobiol. A Chem. 180 (2006) 196–204.
[23] F. Dong, W. Zhao, Z. Wu, Nanotechnology 19 (2008) 365607–365616.
[24] X.B. Chen, C. Burda, J. Phys. Chem. B 108 (2004) 15446–15449.
[25] R.S. Ningthoujam, V. Sudarsan, R.K. Vatsa, R.M. Kadam, Jagannath, A. Guptad, J. Alloys Compd. 486 (2009) 864–870.
[26] G. Lakshminarayana, H.C. Yang, J.R. Qiu, J. Alloys Compd. 475 (2009) 569–576.
[27] J.G. Yu, B. Wang, Appl. Catal. B Environ. 94 (2010) 295–302.
[28] R. Long, N.J. English, Chem. Phys. Lett. 478 (2009) 175–179.
[29] B.J. Morgan, G.W. Watson, J. Phys. Chem. C 113 (2009) 7322–7328.
[30] G. Mattioli, F. Filippone, P. Alippi, A.A. Bonapasta, Phys. Rev. B 78 (2008) 24201–24204.
[31] R. Long, Y. Dai, B. Huang, J. Phys. Chem. C 113 (2009) 650–653.
[32] J. Graciani, J.F. Sanz, A.M. Marquez, J. Phys. Chem. C 113 (2009) 930–938.
[33] G.Z. He, M.Y. Zhang, G. Pan, J. Phys. Chem. C 113 (2009) 21679–21686.
[34] W. Wei, Y. Dai, M. Guo, L. Yu, B.B. Huang, J. Phys. Chem. C 113 (2009) 15046–15050.
[35] M. Miyauchi, M. Takashio, H. Tobimatsu, Langmuir 20 (2004) 232–236.